Appl Phys A (2010) 101: 601–607
DOI 10.1007/s00339-010-5975-7

Applied Physics A
Materials Science & Processing

Electrical characterization of gadolinia-doped ceria films grown by pulsed laser deposition

K. Rodrigo · S. Heiroth · M. Lundberg · N. Bonanos · K. Mohan Kant · N. Pryds · L. Theil Kuhn · V. Esposito · S. Linderoth · J. Schou · T. Lippert

Received: 22 November 2009 / Accepted: 15 June 2010 / Published online: 31 August 2010

Abstract Electrical characterization of 10 mol% gadolinia doped ceria (CGO10) films of different thicknesses prepared on MgO(100) substrates by pulsed laser deposition is presented. Dense, polycrystalline and textured films characterized by fine grains (grain sizes < 18 nm and < 64 nm for a 20-nm and a 435-nm film, respectively) are obtained in the deposition process. Grain growth is observed under thermal cycling between 300 and 800°C, as indicated by X-ray-based grain-size analysis. However, the conductivity is insensitive to this microstructural evolution but is found to be dependent on the sample thickness. The conductivity of the nanocrystalline films is lower (7.0×10^{-4} S/cm for the 20-nm film and 3.6×10^{-3} S/cm for the 435-nm film, both at 500°C) than that of microcrystalline, bulk samples (6×10^{-3} S/cm at 500°C). The activation energy for the conduction is found to be 0.83 eV for the bulk material, while values of 1.06 and 0.80 eV are obtained for the 20-nm film and the 435-nm film, respectively. The study shows that the ionic conductivity prevails in a broad range of oxygen partial pressures, for example down to about 10^{-26} atm at 500°C.

K. Rodrigo (✉) · M. Lundberg · N. Bonanos · K. Mohan Kant · N. Pryds · L. Theil Kuhn · V. Esposito · S. Linderoth
Fuel Cells and Solid State Chemistry Division, Risø DTU, Technical University of Denmark, 4000 Roskilde, Denmark
e-mail: kata@risoe.dtu.dk
Fax: +45-46775858

S. Heiroth · T. Lippert
General Energy Research Department, Paul Scherrer Institute, 5232 Villigen PSI, Switzerland

J. Schou
Department of Photonics Engineering, Risø Campus, Technical University of Denmark, 4000 Roskilde, Denmark

1 Introduction

The development of low temperature solid oxide fuel cells (LT-SOFCs) is believed to support the SOFC technology in entering the energy market. In order to reach this goal, two strategies are applied to lower internal resistive losses yielding access to the lower operation temperatures at reasonable cell performances. Firstly, electrolyte materials with enhanced ionic conductivity, such as rare-earth-doped ceria (CeO_2–Re_2O_3), e.g. 10 mol% Gd_2O_3 doped CeO_2 (CGO10), are applied instead of the conventionally used 8 mol% yttria stabilized zirconia (8YSZ) [1–4]. Secondly, thin-film technologies are employed to reduce the electrolyte thickness to the sub-μm level, as the ohmic resistance scales linearly with the thickness. However, it was shown that transport properties of thin ceria-based electrolytes depart vastly from bulk, microcrystalline materials [5–13]. For example, a wide range of conductivity levels (from 3.4×10^{-6} S/cm [12] to 7×10^{-3} S/cm [8], both at 500°C) and a significant variation of activation energy (from 0.81 eV [10] to 1.3 eV [9]) have been reported. Moreover, n-type conductivity, developing under reducing conditions, can be observed at higher oxygen partial pressure than in bulk materials ($\sim 10^{-15}$ atm at 600°C for thin films [8, 9], compared to $\sim 10^{-22}$ atm at 600°C for bulk materials [5, 14]). In addition, the performance of the thin electrolytes might suffer from structural instability, likely related to the low film density [7, 15]. In this context, the investigation of optimal structural and transport properties of thin CGO10 films is of importance. Furthermore, as the thin-film LT-SOFC designs show different trends regarding the electrolyte film thickness (very thin ∼50 nm [21] or thicker ∼500 nm [18–20] electrolytes are applied), thickness-dependent properties of the CGO10 films also need to be investigated.

The aim of this study is to investigate the transport properties of two CGO10 films deposited for 5 min and 120 min, resulting in approximate thicknesses of 20 and 435 nm. The films are prepared by pulsed laser deposition (PLD), a versatile technique that allows for film-density adjustment [15, 16]. PLD is expected to find large-scale industrial applications [17] and has already been utilized for preparing thin electrolytes in micro-SOFCs [18–21]. Electrical characterization of dense, nanocrystalline and textured CGO10 films prepared on MgO(100) substrates is studied by impedance spectroscopy and DC measurements.

2 Experimental procedure

Thin films were prepared by the PLD technique in a vacuum chamber with a base pressure of 10^{-6} mbar. An excimer laser beam at a wavelength of 248 nm, a pulse length of 20 ns, 350 mJ direct output energy and 10 Hz repetition rate was focused to a spot of 0.036 cm^2 on a rotating target. The target was prepared from commercial CGO10 powder provided by Rhodia, by pressing in a uniaxial (2 tons for 1 min) and in an isostatic press (60 tons for 0.5 min) and by sintering at 1500°C for 12 h. The laser fluence on the target was 1.1 J/cm^2. The pressure of the oxygen background gas was kept at 10^{-2} mbar. The laser-ejected material was collected on substrates placed at a distance of ∼68 mm from the target. Single-crystal MgO(100) substrates used in the experiments were cleaned in ethanol prior to the depositions. The temperature of the substrates was kept at 400°C. The films were deposited for 5 and 120 min, leading to the film thicknesses of 20 and 435 nm, respectively.

The thickness and structure of the nanocrystalline films were analyzed by a scanning electron microscope (SEM, Zeiss Supra) equipped with a field-emission gun. The micrographs were obtained by an in-lens detector.

The crystallographic phase and film orientation of the as-prepared and heat-treated films were obtained by X-ray diffraction (XRD) using a STOE diffractometer with Cu-K_α radiation. Typically, θ–2θ XRD scans were obtained in the 2θ range of 20–90 deg with a resolution of 0.05 deg/step and 5 s integration time per step. Following the outline given in [22], the XRD analysis leading to grain-size estimation was performed. Single-line analysis, performed using the OriginPro7.5 software, with pseudo Voigt peak shapes was used to calculate the peak positons and the internal breadths β. For each Bragg reflection a linear background was subtracted. The average grain size was estimated by the Scherrer equation with a Cauchy type of line shape. The internal breadth of the instrument (0.15 ± 0.02 deg) was measured using a LaB_6 NIST standard 660.

The 'in-plane' electrical characterization of the films was performed by impedance spectroscopy. Sputtered silver electrodes of about 400-nm thickness and 5 mm apart were contacted with Ag paste and Pt wires for all experiments. A Hioki 3250-50 frequency response analyzer in the 42 Hz–1 MHz frequency range and a Solartron 1260 in the 0.01 Hz–2 MHz frequency range were employed for the electrical characterization. An excitation amplitude (RMS) of 0.5–3 V applied to the samples yielded coinciding impedance spectra, indicating linear response to the electrical signal. The conductivity measurements were performed in an air flow of 10 ml/min and in a temperature range of 300–700°C (435-nm film) or of 450–800°C (20-nm film) with a 2°C/min heating and cooling rate, and 30 min dwell time before each measurement. Multiple heating and cooling cycles were applied, in order to validate the electrical sample stability. For comparison, continuous two-point DC measurements were performed with a 5°C/min ramp rate by a Keithley 2700 multimeter. An YSZ oxygen sensor was used to monitor the partial pressure of oxygen, while O_2, air, N_2 and mixtures of N_2 and N_2/H_2 (9%) in 1% H_2O were supplied to the furnace during the oxidation–reduction cycling.

Impedance spectroscopy, in a 250–600°C temperature range, was also undertaken on a bulk CGO10 pellet. Silver electrodes were painted on both sides of the pellet and baked out for 1 h at 600°C in order to remove organic residues. All impedance data were analysed using the ZSimpWin 3.21 software [23].

3 Results

An example of the structural characteristics of the as-prepared and thermally treated films is presented in Fig. 1. The plan view and the cross-sectional SEM micrographs reveal densely packed columnar structures without visible porosities or cracks. Figure 1a presents the as-prepared film, whereas Fig. 1b depicts the film after thermal cycling in the conductivity measurements. It is worth noticing that thermal treatment and extended oxidation–reduction cycling do not influence the film–substrate adhesion. Moreover, no significant microstructural evolution of the film is observed (see the insets in Fig. 1).

A summary of the film' crystallographic properties is depicted in Fig. 2. Figure 2a shows the variation of the films' texture, inferred from XRD spectra. The orientation of the as-deposited and thermally cycled films is presented and compared with a randomly oriented powder sample. The temperature-driven texture evolution is observed in both polycrystalline films. The 20-nm film is initially mainly {111} textured, and it develops a variety of orientations within the thermal cycling time. The 435-nm film transforms from polycrystalline with dominating {111} texture at the as-deposited state to predominantly {200} oriented after the heat treatment. Figure 2b presents the grain sizes derived from Bragg reflections for the as-prepared and thermally cycled films. Thermally activated coarsening of grains is observed in the films. The grains grow at the expense of each

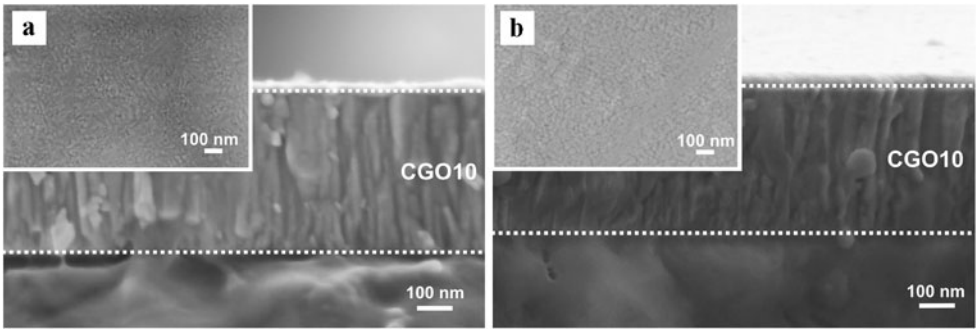

Fig. 1 SEM micrographs of 435-nm (**a**) as-deposited and (**b**) thermally treated films. Cross-sectional images are obtained on fractured samples. *Insets*: plan-view micrographs of the films

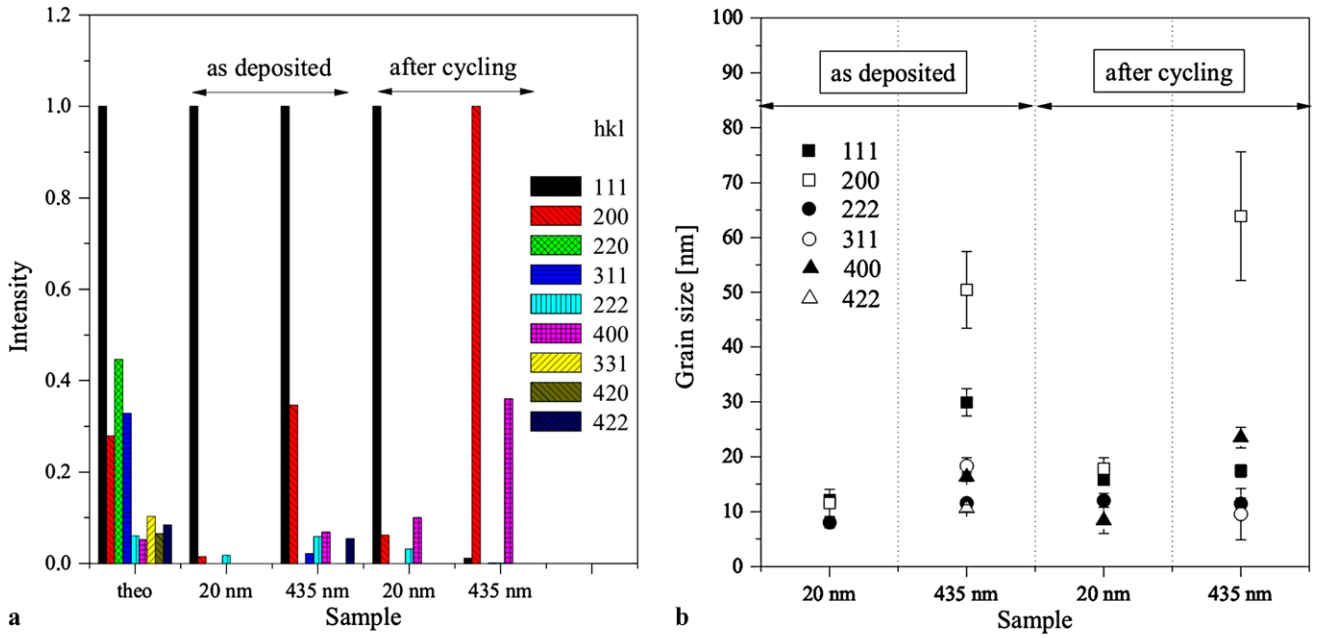

Fig. 2 (**a**) Comparison of CGO10 film texture with randomly oriented powder sample (theo). Textures of the as-deposited films and films subjected to thermal cycling in the conductivity measurements. Graph includes peaks with intensity error <20%. (**b**) Variation of the grain size vs. grain orientation for as-deposited samples and samples thermally cycled in the conductivity measurement. Errors estimated by the error propagation method based on errors of peak position and FWHM

other, but in each case the {200}-oriented grains remain the largest: 12 ± 3 nm and 18 ± 2 nm in the as-prepared and the heat-treated 20-nm films, and 50 ± 7 nm and 64 ± 12 nm in the as-prepared and the thermally cycled 435-nm films, respectively.

Figure 3 shows the impedance spectra of a thin (20 nm) polycrystalline CGO10 film. In contrast to bulk polycrystalline samples, typically showing contributions from grain interiors, grain boundaries as well as the electrodes (each of them modelled by a *RC* circuit with resistance (R) and characteristic capacitance (C) connected in parallel [24]), the impedance spectra of the thin films are described by one semicircle represented by a *RC* equivalent circuit. The capacitance value ($\sim 10^{-11}$ F) describing this *RC* circuit is of the order of the stray capacitance of the measuring cell, indicating that the C value might not be characteristic of the film. This fact indicates that the 'in-plane' characterization of the thin films by alternating current may give limited information about the thin sample, i.e. restricted only to the total resistance of the thin electrolyte film. Figure 3 also shows that the real component derived from the impedance spectra and the resistance measured by the two-point DC method are equal and are ascribed to the total resistance of the electrolyte. However, literature data [7, 8, 25, 26] show that equivalent circuit modelling the response of a thin film to an electrical excitation is subject to a variety of interpretations.

The temperature-dependent total electrical conductivity is shown in an Arrhenius plot (Fig. 4) for thin films and bulk material. Figure 4 presents conductivity data obtained within two heating and cooling cycles. It is noteworthy that the multiple thermal cycling has no influence on the conductivity. The conductivity level of the 20-nm film (7.0×10^{-4} S/cm at 500°C) is distinct from bulk CGO10 ($6 \times$

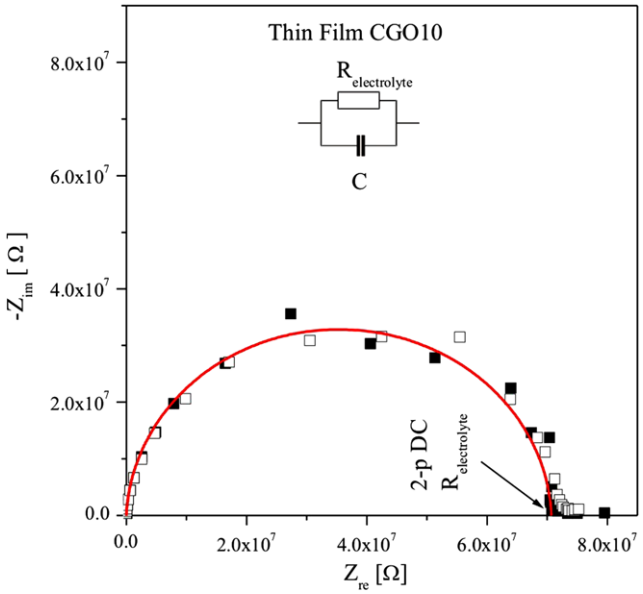

Fig. 3 Impedance spectrum of the 20-nm thin film. The spectrum is obtained at 600°C with RMS = 1 V (*closed symbols*) and 3 V (*open symbols*). The fit to the experimental data (RMS = 1 V) is indicated in the graph. The real part of the impedance spectrum (Z_{re}) assigned to the total resistance of the electrolyte, $R_{electrolyte}$, is the sum of the grain interior (R_{gi}) and grain boundary resistance (R_{gb}), and equals the resistance measured in the two-point DC measurement (2-p DC)

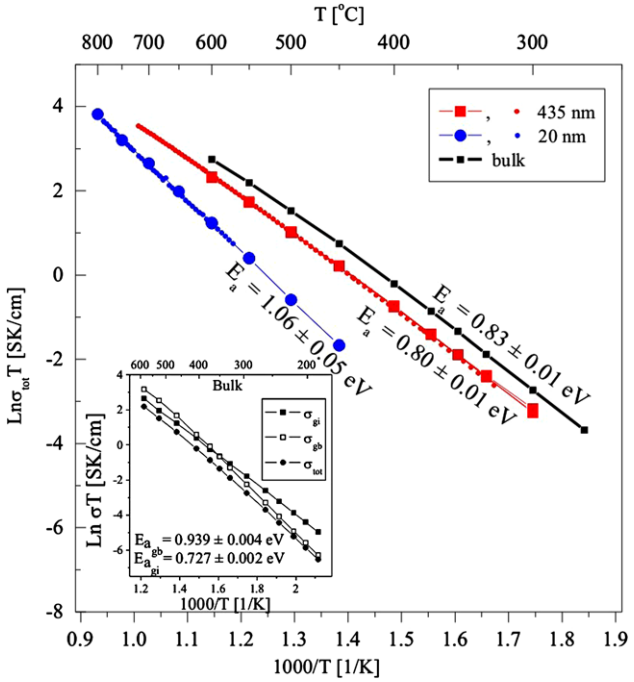

Fig. 4 The total electrical conductivity of CGO10 thin films (20 and 435 nm) in air. Closed symbols indicate total conductivity during the thermal cycling. Large symbols correspond to the impedance measurements, whereas small dots represent two-probe DC measurements. Comparison with conductivity of the bulk CGO10 (*solid line*) is included in the graph. The activation energy (E_a) below 600°C for the conduction in the thin films and the bulk CGO10 is indicated in the graph. Inset: contributions of the grain interior (σ_{gi}) and the grain boundary (σ_{gb}) to the total conductivity (σ_{tot}) of the bulk CG010 material. The activation energy of the grain interior (Ea_{gi}) and the grain boundary (Ea_{gb}) in the 250–600°C temperature range is indicated in the inset. Errors of the activation energy are based on the errors of the geometrical factor L/A for each sample

10^{-3} S/cm at 500°C), whereas the conductivity of the 435-nm film (3.6×10^{-3} S/cm at 500°C) approaches the bulk value. The activation energy of both thin films, derived from the Arrhenius plots, i.e. ln σT vs. $1/T$, varies. The activation energy for the 435-nm film is $E_a = 0.80 \pm 0.01$ eV, whereas a relatively high activation energy is obtained for the 20-nm film, i.e. $E_a = 1.06 \pm 0.05$ eV. For comparison, the activation energy of bulk CGO10 is presented. It equals 0.83 ± 0.01 eV in the 250–600°C temperature range, where the contribution from the grain interior results in 0.727 ± 0.002 eV and from the grain boundary results in 0.939 ± 0.004 eV (see inset in Fig. 4).

The 435-nm film was chosen to study transport behavior in reducing conditions, as the higher conductivity makes it a potentially better electrolyte choice for LT-SOFC applications. The total electrical conductivity (σ_{tot}) of the film was investigated in a broad range of oxygen partial pressures (pO_2) and temperatures (Fig. 5). In the high-and intermediate-pO_2 regimes σ_{tot} is pO_2 independent, whereas in the low-pO_2 region σ_{tot} increases. This relationship is given by the equilibrium condition between the solid oxide (film) and the gas phase, that induces the oxygen depletion and an increase in the concentration of electronic charge carriers, i.e. the reduction of the Ce^{+4} to Ce^{+3}, in the solid oxide, as pO_2 decreases. At high pO_2 the ionic component, determined by the doping level [3, 4], dominates in the electrical conductivity (plateau in the σ_{tot} vs. pO_2 plot). In Fig. 5a, where the 435-nm film is compared with bulk materials, one can notice that the range of the dominant ionic conduction in the 435-nm film is similar to the bulk microcrystalline CGO10 and CGO20 [5, 14]. The ionic conduction of the film prevails down to $\sim 10^{-32}$ atm at 400°C, $\sim 10^{-26}$ atm at 500°C and $\sim 10^{-22}$ atm at 600°C. The domination of the electronic defects in the low-pO_2 region is expressed in a distinct $pO_2^{-1/n}$ dependence. The value of the exponent $-1/n$ yields $-1/4$ or $-1/6$ depending on the doping regime [3, 4]. The value of the exponent for the 435-nm film (see Fig. 5b) is not clear, as the extent of the experimental points at the knee of the $pO_2^{-1/n}$ dependence is narrow.

4 Discussion

The development of polycrystalline CGO10 films on MgO(100) substrates (see Fig. 2) can be explained by the large lattice mismatch characterizing the MgO/CGO10 system, i.e. 29% relative lattice mismatch in the case of the cube on cube growth ($a_{CGO10} = 5.418$ Å [27], $a_{MgO} = 4.211$ Å

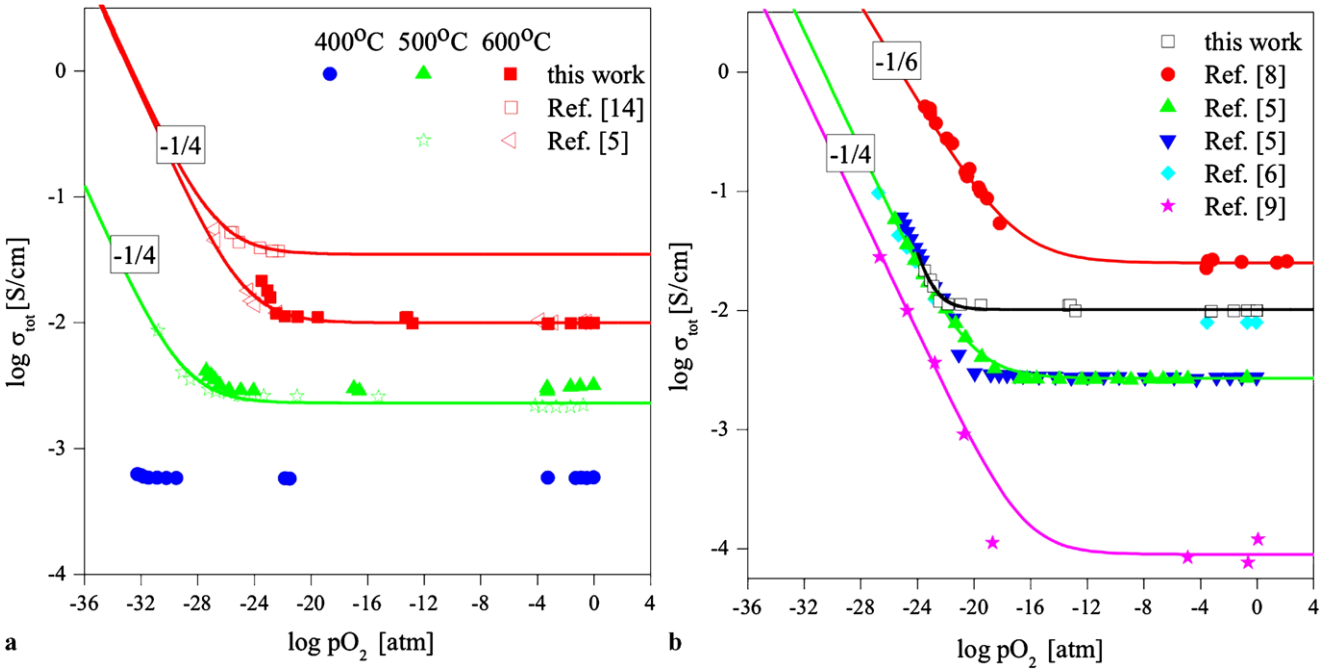

Fig. 5 The total conductivity (σ_{tot}) as a function of the oxygen partial pressure (pO_2). (**a**) Comparison of the extent of predominantly ionic conductivity for 435-nm film (this work) and bulk data: CGO10 [14] and CGO20 [5]. *Solid lines* are drawn as eye-guides. The exponent $-1/4$ is indicated for the bulk data. (**b**) Comparison of σ_{tot} vs. pO_2 dependence at 600°C for 435-nm film (this work) with thin-film data from the literature: CSO20 [8], CGO20 [5], CGO20 [5], CGO20 [6] and CGO20 [9]. The *solid lines* are drawn as eye-guides. Reported literature values of exponents, i.e. $-1/4$ and $-1/6$, are indicated in the graph

[28]), that impedes the epitaxial film growth. In addition,the growth of polycrystalline grains might be enhanced by the atomically rough MgO surface [29].

The nanocrystalline, columnar microstructure (see Figs. 1 and 2) of the CGO10 films implies a high sensitivity to grain-boundary effects in the 'in-plane' electrical measurement geometry, since the direction of the charge-carrier transport is perpendicular to the main axis of the columnar grains. This effect cannot be however directly derived from the conductivity measurements (see Fig. 3), but it can be anticipated from the XRD data (see Fig. 2), i.e. from the relationship between the film thickness and the film grain size. The influence of the grain-boundary contribution on the electrical performance of the films increases with the refinement of the grain sizes. This effect is thus expected to be most pronounced in the 20 nm film with high grain interface density, as evidenced by the small grain sizes (see Fig. 2b). Accordingly, the film activation energy (1.06 eV) is significantly higher than the grain interior activation energy found for the microcrystalline bulk CGO10 (0.727 eV). The low conductivity of the film indicates blocking nature of the grain boundaries, in accord with the report by Chiang et al. [30]. In the 435-nm film, the ionic transport character changes due to the smaller grain interface density indicated by larger grain sizes (see Fig. 2b). Consequently, the conductivity of the 435-nm film increases and approaches the total conductivity of the bulk CGO10. The film activation energy (0.80 eV) resembles the overall activation energy of the bulk microcrystalline CGO10 (0.83 eV). However, the grain interface density cannot explain the observed transport properties alone, as thermally activated grain size evolution is observed (see Fig. 2b) and does not affect the conductivity of the films (see Fig. 4). Further explanation is given by the relationship between the material microstructure in the film–substrate interface and the film conductivity. Although the exact mechanism for the oxygen conduction within interfaces is not yet fully understood [31–33], the investigation of the conduction of thin (10–20 nm range) YSZ prepared on MgO(100) in a polycrystalline [31] and epitaxial [32] form indicates that the interfacial crystallographic faults developing in order to accommodate the film material on the substrate can lead to oxygen-diffusion blocking, resulting in deteriorated transport characteristics [31]. This effect, pronounced in the case of the 20-nm film, relaxes in the 435-nm film, as the interfacial crystallographic faults are averaged over a thickness of ~800 unit cells compared to ~40 unit cells in the case of the 20-nm thin film. However, this aspect of thin-film conduction has to be further investigated, in order to clarify the observed variations.

The σ_{tot} vs. pO_2 dependence indicates that the 435-nm film displays characteristics comparable with bulk material. However, in thin films prepared by various methods and

at different deposition conditions this performance is subjected to a significant variation (see Fig. 5b) often related to the grain size dependent properties of ceria-based materials [5, 9]. For example, despite the large scattering of the conductivity values, one can notice that at 600°C the predominantly ionic conductivity can be found between $\sim 10^{-22}$ atm [6] and $\sim 10^{-15}$ atm [8, 9] (a value that is obtained at ~800°C in bulk, microcrystalline CGO10 [14]). Moreover, Fig. 5a indicates that in bulk materials a $-1/4$ exponent is followed at low temperatures but a change of defect chemistry in thin films (see Fig. 5b), exemplified by a change of the $-1/n$ exponent from $-1/4$ [5, 6, 9] to $-1/6$ [8] (a value that can be seen in bulk CGO10 only at ~1000°C [4]), can be observed. No evidence for such departure from defect chemistry characteristic of bulk materials can be anticipated in our case.

Despite the multiple thermal treatments during conductivity characterization, a stable electrical performance of both films was obtained. In our opinion, this is primarily due to the high density of the as-deposited films, as the conductivity variations are often related to the low film density [7, 15]. In addition, in our study, no relationship between grain size and electrical response can be found, as the thermally induced grain evolution does not affect the conductivity of the films. Although this is in disagreement with other reports [9, 11] which relate conductivity and grain size (boundary density) in the nano-grained materials, no agreement in this topic has been reached so far [30, 34]. Moreover, no relationship between film texture and film conductivity was found. To our knowledge, there exists no report in the literature on this subject for ceria-based films. However, Sanna et al. [8] indicated that highly textured (epitaxial) films (~400-nm thickness) are more structurally stable in the oxidation–reduction cycling, i.e. no microstructural degradation resulting in open porosities or film delamination is observed. Neither of these structural features was seen in our case (see Fig. 1b), indicating that texture might not be a major player in the films' structural stability.

5 Conclusions

The temperature- and oxygen-dependent transport properties of CGO10 electrolyte films prepared by the PLD technique on MgO(100) substrates were investigated. Under extended thermal treatment in the conductivity measurements, nanocrystalline and textured films undergo structural reorganization, characterized by grain coarsening and crystallographic reorientation. These two factors have no influence on the conductivity of the samples, which is likely due to the high density of the as-prepared films. The conductivity and the activation energy are affected by the film thickness (lower conductivity and higher activation energy in the 20-nm film). This is explained by the strong effect of microstructural complexity at the film–substrate interface and the differences in the grain-boundary density in both films. The 435-nm film displays transport properties similar to bulk materials due to decreased grain-boundary contribution and the smaller effect of the film–substrate interface quality.

Acknowledgements The authors would like to acknowledge Finn Saxild and Jørgen Geyti for technical assistance in PLD depositions.

References

1. H. Inaba, H. Tagawa, Solid State Ion. **83**, 1 (1996)
2. J.A. Kilner, Solid State Ion. **129**, 13 (2000)
3. M. Mogensen, N.M. Sammes, G.A. Topsett, Solid State Ion. **129**, 63 (2000)
4. B.C.H. Steele, Solid State Ion. **129**, 95 (2000)
5. J.L.M. Rupp, A. Infortuna, L.J. Gauckler, J. Am. Ceram. Soc. **90**, 1792 (2007)
6. J.H. Joo, G.M. Choi, J. Eur. Ceram. Soc. **27**, 4273 (2007)
7. L. Chen, C.L. Chen, X. Chen, W. Donner, S.W. Liu, Y. Lin, D.X. Huang, A.J. Jacobson, Appl. Phys. Lett. **83**, 4737 (2003)
8. S. Sanna, V. Esposito, D. Pergolesi, A. Orsini, A. Tebana, S. Licoccia, G. Balestrino, E. Traversa, Adv. Funct. Mater. **19**, 1713 (2009)
9. T. Suzuki, I. Kosacki, H.U. Anderson, Solid State Ion. **151**, 111 (2002)
10. L. Chen, C.L. Chen, D.X. Huang, Y. Lin, X. Chen, A.J. Jacobson, Solid State Ion. **175**, 103 (2004)
11. J.L.M. Rupp, L.J. Gauckler, Solid State Ion. **177**, 2513 (2006)
12. G. Chiodelli, L. Malavasi, V. Massarotti, P. Mustarelli, E. Quartarone, Solid State Ion. **176**, 1505 (2005)
13. A. Kathikeyan, M. Tsuchiya, C.-L. Chang, S. Ramanathan, Appl. Phys. Lett. **90**, 263108 (2007)
14. S. Wang, T. Kobayashi, M. Dokiya, T. Hatshimoto, J. Electrochem. Soc. **147**, 3606 (2000)
15. A. Infortuna, A. Harvey, L. Gauckler, Adv. Funct. Mater. **18**, 127 (2008)
16. K. Rodrigo, S. Heiroth, M. Döbeli, N. Pryds, S. Linderoth, J. Schou, T. Lippert, J. Optoelectron. Adv. Mater. **12**, 511 (2010)
17. R. Eason, *Pulsed Laser Deposition of Thin Films: Applications-Led Growth of Functional Materials* (Wiley, New York, 2007)
18. X. Chen, N.J. Wu, L. Smith, A. Ignatiev, Appl. Phys. Lett. **84**, 2700 (2004)
19. A. Bieberle-Hutter, D. Beckel, U.P. Mueckle, J.L. Rupp, A. Infortuna, L.J. Gauckler, Mstnews **04–05**, 12 (2005)
20. S. Rey-Mermet, P. Muralt, Mater. Res. Soc. Symp. Proc. **972**, 10 (2007)
21. H. Huang, M. Nakamura, P. Su, R. Fasching, Y. Saito, F.B. Prinz, J. Electrochem. Soc. B **154**, 20 (2007)
22. M. Birkholz, *Thin Film Analysis by X-ray Scattering* (Wiley, Weinheim, 2006)
23. ZSimpWin 3.21, EChem Software. Bruno Deum, Ann Arbor, Michigan, USA, 1999–2005
24. E. Barsoukov, J. Ross Macdonald, *Impedance Spectroscopy, Theory, Experiment and Applications* (Wiley-Interscience, Hoboken, 2005)
25. I. Kosacki, B. Gorman, H.U. Anderson, ECS Proc. **97**, 631 (1996)
26. T. Petrovski, H.U. Anderson, V. Petrovski, Mater. Res. Soc. Symp. Proc. **756**, 515 (2003)
27. G. Brauer, H. Gradinger, Z. Anorg. Allg. Chem. **276**, 209 (1954)
28. R.W.G. Wyckoff, Z. Kristallogr. **62**, 529 (1925)

29. M.P. Delplancke-Ogletree, M. Ye, R. Winand, J.F. de Marneffe, R. Deltour, J. Mater. Res. **14**, 2133 (1999)
30. Y.M. Chiang, E.B. Lavik, D.A. Blom, Nanostruct. Mater. **9**, 633 (1997)
31. X. Guo, E. Vasco, S. Mi, K. Szot, E. Wachsman, R. Waser, Acta Mater. **53**, 5161 (2005)
32. I. Kosacki, C.M. Rouleau, P.F. Becher, J. Bentley, D.H. Lowndes, Solid State Ion. **176**, 1319 (2005)
33. N. Schichtel, C. Korte, D. Hesse, J. Janek, Phys. Chem. Chem. Phys. **11**, 3043 (2009)
34. R.A. De Souza, M.J. Pietrowski, U. Anselmi-Tamburini, S. Kim, Z.A. Munir, M. Martin, Phys. Chem. Chem. Phys. **10**, 2067 (2008)